Journal of Catalysis 261 (2009) 217–223

Contents lists available at ScienceDirect

Journal of Catalysis

www.elsevier.com/locate/jcat

Mechanism of ammonia oxidation over PGM (Pt, Pd, Rh) wires by temporal analysis of products and density functional theory

Javier Pérez-Ramírez [a,b,*], Evgenii V. Kondratenko [c,*], Gerard Novell-Leruth [a,d], Josep M. Ricart [d]

[a] Institute of Chemical Research of Catalonia (ICIQ), Avinguda Països Catalans 16, 43007, Tarragona, Spain
[b] Catalan Institution for Research and Advanced Studies (ICREA), Passeig Lluís Companys 23, 08010, Barcelona, Spain
[c] Leibniz-Institut für Katalyse e. V. an der Universität Rostock, Außenstelle Berlin Richard-Willstätter-Str. 12, D-12489, Berlin, Germany
[d] Departament de Química Física i Inorgànica, Universitat Rovira i Virgili, C/Marcel.lí Domingo s/n, 43007, Tarragona, Spain

ARTICLE INFO

Article history:
Received 8 October 2008
Revised 19 November 2008
Accepted 23 November 2008
Available online 17 December 2008

Keywords:
NH_3 oxidation
Mechanism
Platinum
Palladium
Rhodium
Wires
TAP reactor
DFT

ABSTRACT

The mechanism of ammonia oxidation over Pt, Pd, and Rh wires has been investigated in the Temporal Analysis of Products (TAP) reactor at relevant temperatures in industrial ammonia burners. The results of primary ($NH_3 + O_2$) and secondary ($NH_3 + NO$) interactions with isotopically labeled ammonia at 1073 K enable to conclude that the overall reaction pathways to NO, N_2O, and N_2 are equivalent on the three noble metals. NO is a primary reaction product, while N_2 and N_2O originate from consecutive NO transformations. The extent of the secondary reactions determines the net NO selectivity. Rhodium is the most active catalyst for the unwanted reduction of NO by NH_3, while platinum shows the lowest activity. This explains the superior NO selectivity attained over Pt and, therefore, its industrial application. The TAP-derived selectivity ranking was substantiated by Density Functional Theory calculations on the (100) facets of the noble metals. We proved experimentally that NO selectivity approaching 100% at complete NH_3 conversion can be equivalently attained over Pt, Pd, and Rh by increasing the oxygen content in the feed. For a feed of $O_2/NH_3 = 10$, both N_2O and N_2 production are suppressed due to the impeded NO dissociation and favored NO desorption at high oxygen coverage.

1. Introduction

The synthesis of ammonia (Haber–Bosch process) and its oxidation (Ostwald process) are two of the most investigated reactions in heterogeneous catalysis from mechanistic and kinetic viewpoints. These processes are in industrial scale since the early 20th century for the production of nitrogenated products such as fertilizers, explosives, and chemical feedstocks. Ammonia oxidation on Pt has been studied for more than 80 years, using a wide variety of specimens, conditions, and methods. Refs. [1–12] cover representative research on the topic in the last four decades. Platinum gauzes are used since the implementation of the Ostwald process on a large scale in the 1920's. The only significant modification of the catalyst occurred in the 1930's when the beneficial effect of rhodium was discovered [13] and led to the Pt–Rh alloys with 5–10% Rh. These alloys operate at 1023–1073 K, achieving NO selectivities >94% and stable performance in campaigns of 3–12 months [14]. In contrast to platinum, experimental and theoretical studies addressing the mechanism of ammonia oxidation over other PGMs (Platinum Group Metals) are scarce. Golodets [15] tested pure metals, alloys, metal carbides, and metal oxides in NH_3 oxidation. However, the reaction temperature was limited to 573 K, i.e. no gas-phase NO was observed in the product mixture, and, therefore, the derived conclusions cannot be extrapolated to the industrial situation.

In 1975, Pignet and Schmidt [3] investigated the kinetics of NH_3 oxidation on Pt, Pd, and Rh wires in a steady-state flow system operating up to 1673 K and total pressures of 0.1–1 Torr. Based on the results of NH_3 and NO decomposition as well as the bimolecular $NH_3 + O_2$ and $NH_3 + NO$ reactions, they concluded that there is a temperature window between 973 and 1273 K where nitric oxide is produced over the three metals, although the maximum NO selectivity obtained was higher for Pt (94%) than for Pd (90%) or Rh (79%). The superior NO selectivity of Pt was related to the wide separation in temperature of the N_2 and NO peaks, while there was much more overlap for Pd and Rh. Similarly, the $NH_3 + O_2$ reaction leading to NO and the $NO + NH_3$ reaction leading to N_2 were shifted in temperature on Pt and overlapped on Pd and Rh. Pignet and Schmidt [3] focused the selectivity discussion on NO and N_2, i.e. N_2O was neither detected nor taken into account. However, nitrous oxide is a harmful product of ammonia oxidation and measures to minimize its emission are being implemented [14].

* Corresponding authors. Faxes: +34 977 920 224, +49 30 6392454.
E-mail addresses: jperez@iciq.es (J. Pérez-Ramírez), evgenii.kondratenko@catalysis.de (E.V. Kondratenko).

0021-9517/$ – see front matter
doi:10.1016/j.jcat.2008.11.018

With the exception of [3], no study attempted to identify mechanistic features that make Pt the catalyst of choice in industry versus other noble metals such as pure Rh, i.e. the second component of the commercial alloy, and Pd, i.e. the main component of the catchment gauze pack for platinum recovery in the ammonia burner and sometimes also present in the primary Pt-based alloy. This fundamental understanding can bring an improved process by changing the type of catalyst (e.g. alloy composition) and/or reaction conditions (e.g. temperature, NH_3/O_2 ratio). This optimization is not incremental taking into account that the catalyst cost is a major expense in nitric acid production and the markedly different and fluctuating PGM prices (currently Pt 849 USD/oz, Rh 1275 USD/oz, and Pd 215 USD/oz [16]).

Herein we have studied the high-temperature ammonia oxidation over Pt, Pd, and Rh wires in the Temporal Analysis of Products (TAP) reactor. Several key features of the TAP reactor make it suited to investigate the mechanism of this reaction on the level of near to elementary steps [9,17,18], e.g. (i) sub-millisecond time resolution, (ii) operation under isothermal conditions, (iii) use of isotopically labeled molecules, and (iv) application of practical catalysts. Moreover, peak pressures can be up to 10^9 times higher than in typical UHV studies, narrowing the pressure gap with respect to ambient pressure studies [18]. The main objective of this work is to determine mechanistic differences between the three metals conferring them a more or less selective behavior. For this purpose, primary interactions between $^{15}NH_3$ and O_2 as well as secondary interactions between $^{15}NH_3$ and NO were investigated at 1073 K using different ammonia:oxygen and ammonia:nitric oxide ratios. TAP experiments were complemented by Density Functional Theory (DFT) simulations in order to gain an improved molecular-level understanding of the reaction. We highlight that increasing the O_2/NH_3 ratio effectively minimizes secondary NO transformations to N_2O and N_2. As a result, NO selectivity approaching 100% at a complete degree of NH_3 conversion is attainable over the PGMs.

2. TAP experiments

Transient experiments were carried out in the TAP-2 reactor system using analogous procedures as those reported elsewhere [9,17]. Platinum (99.99%), palladium (99.95%), and rhodium (99.9%) wires with diameters of 0.1 mm (Pt, Pd) and 0.125 mm (Rh) were purchased from Chempur. Ca. 25 mg of the metal wire in a single rounded piece was loaded in the isothermal zone of the quartz microreactor (40 mm length and 6 mm i.d.) between two layers of quartz particles (sieve fraction 250–350 μm). The sample without any pretreatment was evacuated to 10^{-5} Pa. Thereafter, the following pulse experiments were carried out at 1073 K using isotopically labeled ammonia and an overall pulse size of 10^{16} molecules:

- pump-probe of O_2:Xe = 1:1 and $^{15}NH_3$:Ne = 1:1, using time delays (Δt) in the range of 0.1–2 s;
- pulsing of $^{15}NH_3$–O_2 mixtures ($^{15}NH_3$:O_2:Ne = 10:1:10, 1:1:1, 1:2:1, and 1:10:1);
- pulsing of $^{15}NH_3$–NO mixtures ($^{15}NH_3$:NO:Ne = 1:0.2:1, 1:2:1, and 1:5:1).

In the experiments, Ne (4.5), Xe (4.0), O_2 (4.5), NO (2.5), and $^{15}NH_3$ (99.9% atoms of ^{15}N) were used without further purification. Transient responses were monitored at atomic mass units (AMUs) related to reactants, reaction products, and inert gases at the reactor outlet using a quadruple mass spectrometer (Hiden Analytical HAL RC 301). Along the manuscript, only the isotopically labeled nitrogen atoms (^{15}N) in ammonia and reaction products are highlighted by the respective superscript, while no superscript is used for the most abundant nitrogen isotope. The following AMUs were analyzed: 132 (Xe), 46 (NO_2, $^{15}N_2O$), 45 (^{15}NNO), 44 (N_2O, CO_2), 32 (O_2), 31 (^{15}NO, HNO), 30 (N_2O, NO, $^{15}N_2$), 29 (^{15}NN), 28 (N_2O, N_2), 20 (Ne), 18 (H_2O, $^{15}NH_3$), 17 ($^{15}NH_3$, OH), 16 (O_2, $^{15}NH_3$), and 2 (H_2). For each AMU, pulses were repeated 10 times and averaged in order to improve the signal-to-noise ratio. The concentration of feed components and reaction products was determined from the respective AMUs using standard fragmentation patterns and sensitivity factors.

3. DFT calculations

Calculations were performed with the VASP code [19,20], employing the PW91 functional [21], the inner electrons have been represented by projector augmented wave (PAW) pseudopotentials [22], and the valence monoelectronic states have been expanded in plane-waves with a cut-off energy of 400 eV. The Pt(100), Pd(100), and Rh(100) surfaces were modeled by a two-dimensional slab in a three-dimensional periodic cell generated by introducing a vacuum width of ca. 12 Å in the normal direction to the surface. The slabs contained four metal layers with the target atomic or molecular species (N, O, NO, N_2O, N_2) adsorbed on one side of the slab. Optimized metal–metal interatomic distances for the bulk were used to prevent unlikely forces on the metal atoms. The calculated values (2.82 Å Pt–Pt, 2.80 Å Pd–Pd, and 2.72 Å Rh–Rh) are in reasonable agreement with those determined experimentally (2.77, 2.75, and 2.69 Å, respectively) [23]. We considered the 2×2 unit cell associated with a molecular coverage of 0.25 ML. The 2D Brillouin integrations were performed on a $5 \times 5 \times 1$ grid. The geometry optimization included all degrees of freedom of the adsorbates and the two uppermost metal layers, while the two lowest metal planes were fixed at the optimized bulk geometry.

The adsorption energy (E_{ads}) for each species (X) was computed as the difference between the energy of the adsorbed molecule ($E_{X\text{-surface}}$) and the sum of the energies of the clean surface ($E_{surface}$) and the gas-phase species ($E_{X\text{-gas phase}}$) (Eq. (1)). A negative value of E_{ads} indicates an exothermic chemisorption process:

$$E_{ads} = E_{X\text{-surface}} - E_{surface} - E_{X\text{-gas phase}}. \quad (1)$$

Transition states (TS) were determined using the Nudged Elastic Band methods (NEB and CI-NEB) [24] and the Dimer method [25]. TS geometries were refined until a negligible value of the energy gradients was found using the quasi-Newton algorithm implemented in VASP. A full vibrational analysis was carried out to validate the optimized geometry of the adsorbed species and to determine transition states.

4. Results and discussion

4.1. Temporal analysis of products

4.1.1. Reaction of oxygen and ammonia

In order to derive mechanistic insights into the sequence of products formation in the high-temperature ammonia oxidation over Pt, Pd, and Rh wires, primary interactions of O_2 and $^{15}NH_3$ were investigated by pump-probe experiments using different time delays (Δt) between the pulses. Fig. 1 shows the height-normalized transient responses of O_2, ^{15}NO, $^{15}N_2$, and $^{15}N_2O$ upon pulsing of O_2:Xe = 1:1 and $^{15}NH_3$:Ne = 1:1 with $\Delta t = 0.1$ s at 1073 K. The O_2 response sharply decreases when $^{15}NH_3$ was introduced in the reactor due to the reaction of oxygen species adsorbed on the metals with ammonia. In all cases, reaction products were detected exclusively in the ammonia pulse. Independent of the metal, ^{15}NO appears directly after $^{15}NH_3$ followed by $^{15}N_2O$ and $^{15}N_2$. The shape of the transient responses strongly depends on the catalyst. In contrast to Pt, the responses of ^{15}NO and $^{15}N_2O$ over Rh and Pd are very sharp and shifted to shorter times compared to that of $^{15}N_2$. The shape of the transient responses and

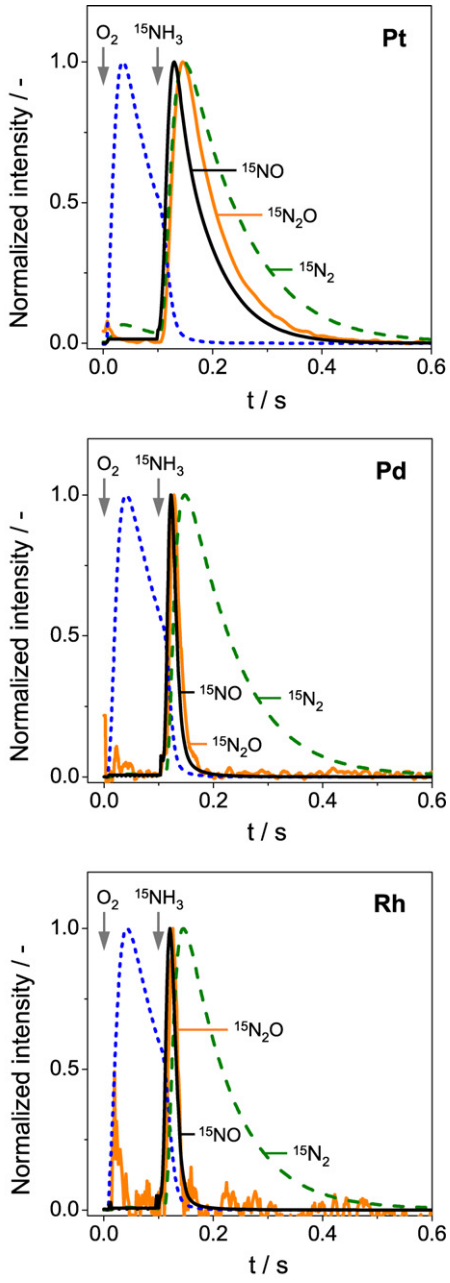

Fig. 1. Normalized transient responses of selected compounds in pump-probe experiments of O_2:Ne = 1:1 and $^{15}NH_3$:Xe = 1:1 ($\Delta t = 0.1$ s) over the metal wires at 1073 K.

their order of appearance provide important mechanistic and kinetic information on chemical and transport phenomena inside the reactor [26]. In the present study, the responses of ^{15}NO, $^{15}N_2O$, and $^{15}N_2$ were quantified by (i) the time of maximum (t_{max}) and (ii) the width at half-height ($t_{h/2}$). These characteristics are shown in Fig. 2. For the three metals, the t_{max} and $t_{h/2}$ follow the order $^{15}N_2 > {}^{15}N_2O > {}^{15}NO$. This indicates that nitric oxide is a primary product of ammonia oxidation, followed by its consecutive transformation into nitrous oxide and dinitrogen. The latter product could also originate from nitrous oxide, by direct decomposition or by reduction with ammonia.

Although the same general scheme of ammonia oxidation seems to be valid for the PGMs, their activities for NO production and its secondary transformations are markedly different. The t_{max} and $t_{h/2}$ values of ^{15}NO are related to the intrinsic rates for its formation from ammonia oxidation and its transformation into nitrous oxide and dinitrogen: the lower these characteristic times, the higher the rates of both processes. The t_{max} of ^{15}NO over Pt, Pd, and Rh were 0.129, 0.122, and 0.120 s, respectively (Fig. 2). The accuracy in t_{max} is ± 0.001 s due to the millisecond resolution of the TAP technique [18,26]. Similarly, the $t_{h/2}$ of the ^{15}NO was significantly higher over Pt than over Pd and Rh, which points to the lower activity of Pt for secondary reactions involving nitric oxide. Analogous dependences of the t_{max} and $t_{h/2}$ are valid for $^{15}N_2O$ and $^{15}N_2$ (Fig. 2). It should be also highlighted that not only the absolute values of t_{max} and $t_{h/2}$ are function of the noble metal, but also the difference between these values of ^{15}NO and $^{15}N_2O$ as well as of $^{15}N_2O$ and $^{15}N_2$. The difference between the t_{max} (or $t_{h/2}$) of ^{15}NO and $^{15}N_2O$ decreases in the order Pt < Pd ~ Rh. The same trend applies to the difference between t_{max} (or $t_{h/2}$) of $^{15}N_2O$ and $^{15}N_2$. This order reflects the activity of the noble metals for secondary transformations of nitric and nitrous oxides into molecular nitrogen.

The above conclusion can also be supported by the $^{15}NH_3$ conversion and the amount of ^{15}NO formed over the catalysts (Fig. 3). When O_2 and $^{15}NH_3$ were sequentially pulsed with $\Delta t = 0.1$ s, the mole fraction of ^{15}NO over Pt, Pd, and Rh was 16.3, 3.4, and 2.1%, respectively. The highest ^{15}NO production over Pt confirms its lower ability for secondary transformations of nitric oxide compared to Pd and Rh. The conversion of ammonia slightly decreased (by ca. 15%) upon increasing the time delay between the O_2 and $^{15}NH_3$ pulses from 0.1 to 2 s. The dependence of the nitric oxide production on the time delay is more pronounced. In fact, the ^{15}NO production dropped to zero over the three catalysts when $\Delta t \geqslant 0.5$ s. Since the conversion of ammonia is practically independent of the time delay between O_2 and $^{15}NH_3$ while the opposite holds for the ^{15}NO production, it is concluded that the oxygen coverage strongly influences secondary transformations of nitric oxide.

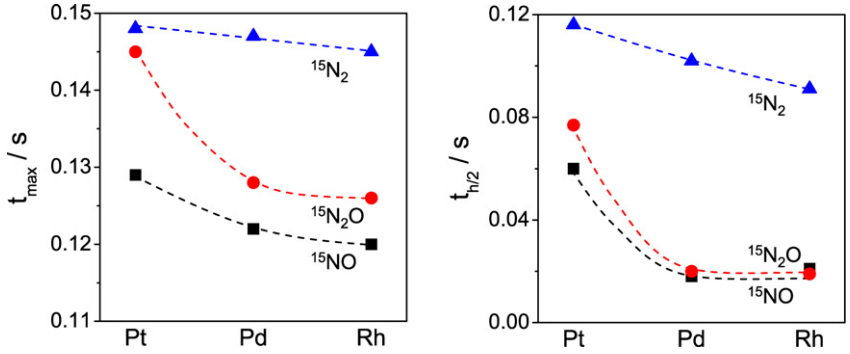

Fig. 2. Characteristic times (t_{max} and $t_{h/2}$) of reaction products over the PGMs derived from the transient responses in pump-probe experiments of Fig. 1.

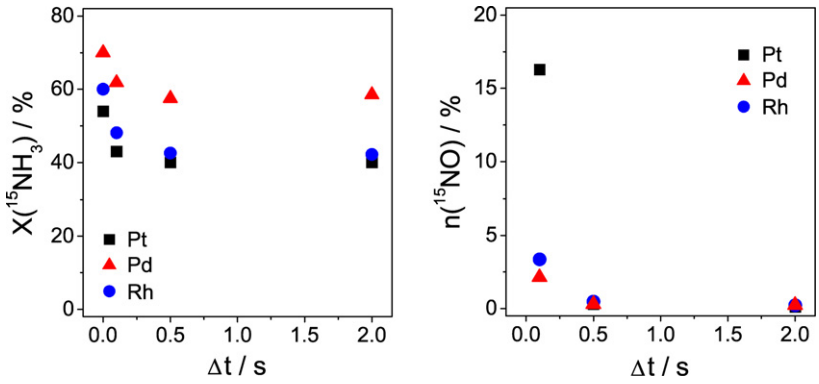

Fig. 3. Conversion of $^{15}NH_3$ (left) and outlet mole fraction of ^{15}NO (right) over the PGMs in pump-probe experiments of O_2:Ne = 1:1 and $^{15}NH_3$:Xe = 1:1 at different time delays and 1073 K.

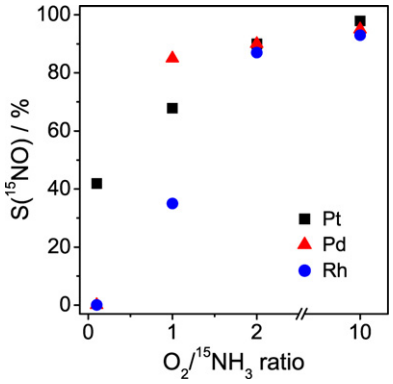

Fig. 4. ^{15}NO selectivity over the PGMs on pulsing of $^{15}NH_3$:O_2:Ne mixtures with different oxygen-to-ammonia ratio at 1073 K.

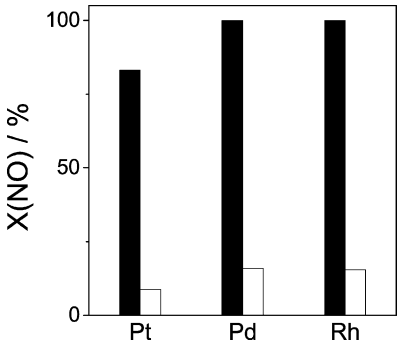

Fig. 5. Conversion of NO over the PGMs on pulsing of $^{15}NH_3$:NO:Ne = 1:0.2:1 (solid bars) and $^{15}NH_3$:NO:Ne = 1:2:1 (open bars) at 1073 K.

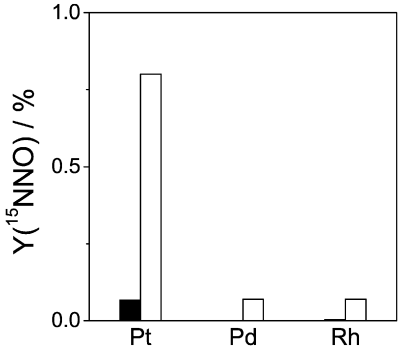

Fig. 6. Yield of ^{15}NNO over the PGMs on pulsing of $^{15}NH_3$:NO:Ne = 1:0.2:1 (solid bars) and $^{15}NH_3$:NO:Ne = 1:2:1 (open bars) at 1073 K.

The dependence of ^{15}NO selectivity on the molar $O_2/^{15}NH_3$ ratio in Fig. 4 supports the role of oxygen coverage in nitric oxide production and its further transformations. The ^{15}NO selectivity strongly increases with an increase in the ratio from 0.1 to 10 over the metals. At $O_2/^{15}NH_3 = 0.1$, the ^{15}NO selectivity over Pt (45%) is much higher than over Pd and Rh (practically zero). Noteworthy, ca. 100% selectivity to nitric oxide was equivalently achieved over the three PGMs at $O_2/^{15}NH_3 = 10$. In the same line, pilot studies by Heck et al. [27] reported nearly 100% NO selectivity for ammonia oxidation with an O_2/NH_3 ratio ca. 3 over $Pt_{0.9}$–$Rh_{0.05}$–$Pd_{0.05}$ gauze.

4.1.2. Reaction of ammonia and nitric oxide

Secondary transformations of nitric oxide into nitrogen and nitrous oxide were studied by pulsing of $^{15}NH_3$/NO mixtures with different composition. Fig. 5 compares the NO conversion over the Pt, Pd, and Rh wires at 1073 K upon pulsing of $^{15}NH_3$/NO mixtures with ratios of 5 and 0.5. Since the mixtures differ in their reducing potential, the relative contribution of the NO reduction by $^{15}NH_3$ versus the direct NO decomposition to the overall activity can be established. For all PGMs, the degree of NO conversion strongly decreases upon decreasing the $^{15}NH_3$/NO ratio. Pt, Pd, and Rh were not active for direct NO decomposition under the applied experimental conditions, i.e. the presence of ammonia was required in order to attain high NO conversion. However, it is important to stress that both Pd and Rh were more active for reduction of nitric oxide by ammonia than Pt.

The present study provides mechanistic insights into nitrous oxide formation, which was not considered in previous kinetic studies of ammonia oxidation comparing Pt, Pd, and Rh [3]. The exclusive formation of ^{15}NNO over all the noble metals applied independent of the ratio of $^{15}NH_3$/NO should be stressed, i.e. this product originates from the coupling of NO and NH_x species. Among the three PGMs, platinum produces relatively more nitrous oxide than palladium and rhodium (Fig. 6). This observation is also valid for $^{15}NH_3$/NO mixtures varying in the ratio from 5 to 0.5. As demonstrated in Fig. 7, the outlet concentration of ^{15}NNO decreases with an increase in the inlet concentration of $^{15}NH_3$, while it increases with an increase in the inlet concentration of NO.

4.2. Density functional theory

In order to substantiate the observations from TAP reactor studies, the reaction pathways leading to NO, N_2O, and N_2 over the (100) surfaces of the three noble metals were analyzed by DFT calculations. Recently, DFT simulations have been used to assess the mechanism of ammonia oxidation on Pt(100) [12], Pt(111) [28], and Rh(111) [29]. These works concluded that the reaction proceeds via an *imide* mechanism, in which NH_3 is progressively dehydrogenated by adsorbed O or OH species and the resulting N atom

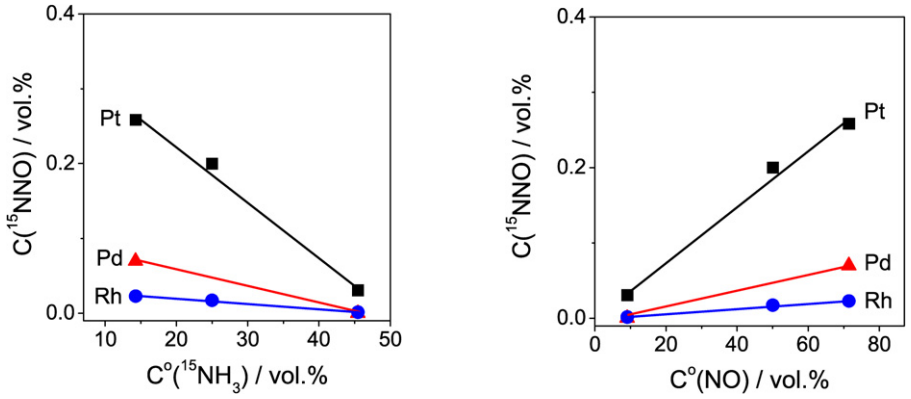

Fig. 7. Outlet concentration of ^{15}NNO over the PGMs on pulsing of $^{15}NH_3$:NO:Ne mixtures as a function of the inlet concentration of ammonia (left) and nitric oxide (right) at 1073 K.

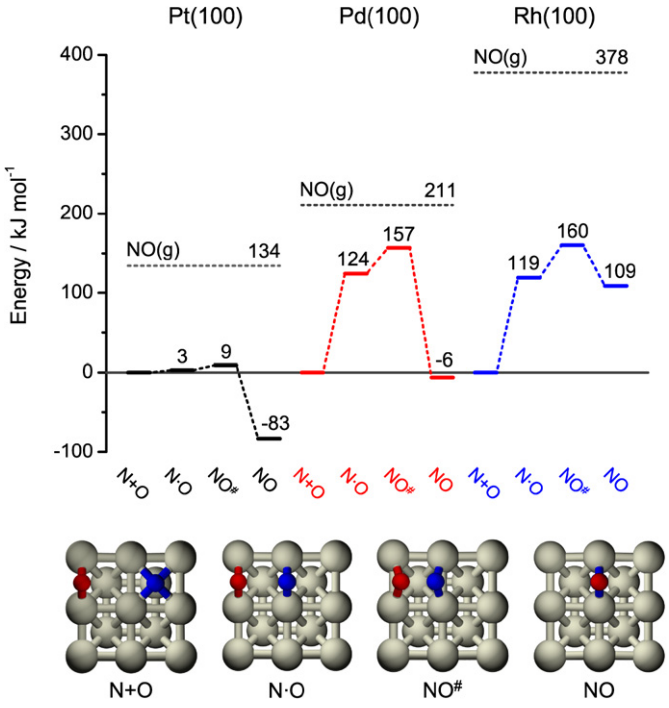

Fig. 8. Pathway of NO formation by reaction of N and O over Pt(100), Pd(100), and Rh(100) at 0.25 ML. Horizontal dashed lines indicate the energy level of gas-phase NO with respect to adsorbed NO on each metal. The bottom schemes illustrates the initial, transition, and final states on Pt(100). The red sphere represents O and the blue sphere represents N. (For interpretation of the references to color in this figure legend, the reader is referred to the web version of this article.)

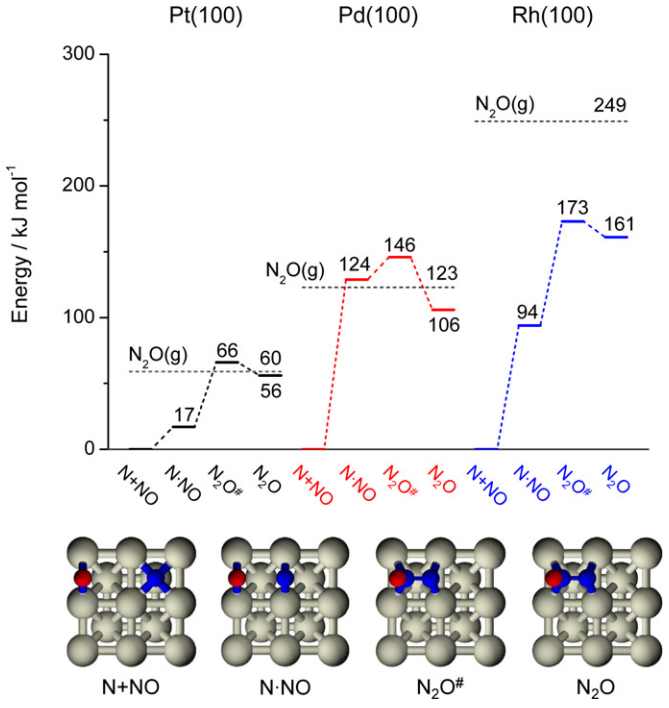

Fig. 9. Pathway of N_2O formation by reaction of N and NO over Pt(100), Pd(100), and Rh(100) at 0.25 ML. Horizontal dashed lines indicate the energy level of gas-phase N_2O with respect to adsorbed N_2O on each metal. The bottom schemes illustrate the initial, transition, and final states on Pt(100). The red sphere represents O and the blue sphere represents N. (For interpretation of the references to color in this figure legend, the reader is referred to the web version of this article.)

leads to reaction products according to Eqs. (2)–(4). Therefore, the calculations in this paper focus on these selectivity-directing steps:

$$N + O \rightarrow NO, \quad (2)$$

$$N + NO \rightarrow N_2O, \quad (3)$$

$$N + N \rightarrow N_2. \quad (4)$$

Figs. 8 and 9 show the energy profiles of NO and N_2O formation over Pt(100), Rh(100), and Pd(100). The energy of the non-interacting reactants (N + O or N + NO) in their most stable position was taken as a common reference, which enables to properly compare the different metals. In agreement with previous calculations over the (100) plane [12,30–32], N and NO occupy hollow and bridge positions on the three metals, respectively. Atomic oxygen adsorbs on bridge sites of Pt(100) and on hollow sites of Rh(100) and Pd(100) at 0.25 ML. The reaction to NO is initiated with the approach of N and O to each other leading to the N·O state, in which both fragments are in bridge position (Fig. 8, bottom scheme). This involves a change of adsorption site from the non-interacting to the coadsorbed states. The energy cost of repositioning adsorbates is 3 kJ mol^{-1} for Pt(100), contrasting with 124 kJ mol^{-1} for Pd(100) and 119 kJ mol^{-1} for Rh(100). The marked difference is due to the much higher stability of N in hollow sites compared to bridge sites on Rh and Pd, being very similar on Pt (Table 1). In addition, the change of oxygen from hollow to bridge on Pd and Rh also contributes to the energy cost, while O_{bridge} is the most stable position on Pt. The activation energy of the reaction N·O → NO$^{\#}$ is significantly lower on platinum (6 kJ mol^{-1}) than on palladium (33 kJ mol^{-1}) and rhodium (41 kJ mol^{-1}). The same conclusion can be extracted from the reaction barrier, which is defined as the energy difference

Table 1
Adsorption energy (kJ mol^{-1}) of atomic N and O in bridge and hollow sites of the PGMs.

Species	Pt(100)		Pd(100)		Rh(100)	
	Bridge	Hollow	Bridge	Hollow	Bridge	Hollow
N	−421	−427	−379[a]	−490	−498	−565
O	−410	−366	−391	−423	−494	−515

[a] Saddle point.

between the non-interacting system (N + O) and the transition state (NO$^{\#}$). This definition lumps the surface diffusion (adsorption site repositioning) and reaction steps and amounts to 9, 157, and 160 kJ mol^{-1} for Pt(100), Pd(100), and Rh(100), respectively. Desorption of NO to the gas phase is clearly the most energy demanding step, i.e. 217 kJ mol^{-1} on Pt(100) and Pd(100), and 269 kJ mol^{-1} on Rh(100). Besides, for selectivity aspects, it is important to stress the significantly lower activation energy of NO dissociation (NO → N·O) on Rh(100) (51 kJ mol^{-1}) compared to Pt(100) (92 kJ mol^{-1}) and Pd(100) (163 kJ mol^{-1}). It is well known that NO dissociation on Rh is much easier than on Pd and Pt [33,34].

The energy profiles of N_2O formation on Pt(100), Rh(100), and Pd(100) by reaction of atomic nitrogen with nitric oxide are shown in Fig. 9. Atomic nitrogen can derive from ammonia dehydrogenation and/or from dissociation of adsorbed NO at low coverage by oxygen species. Similarly to the case in Fig. 8, the approach of N and NO to the coadsorbed state (N·NO) is much more energy demanding on Pd(100) and Rh(100) than on Pt(100) due to the required change of the N adsorption site from hollow to bridge. The activation energy of the reaction N·NO → $N_2O^{\#}$ was 49 kJ mol^{-1} on Pt(100), 22 kJ mol^{-1} on Pd(100), and 79 kJ mol^{-1} on Rh(100). In contrast to NO, desorption of N_2O from the PGM surfaces is much easier. The adsorption energy of N_2O on Pt(100) and Pd(100) is 4 and 17 kJ mol^{-1}, respectively, and a somewhat higher value was computed on Rh(100) (88 kJ mol^{-1}). The higher activation energy over rhodium can partially explain the lower N_2O yield observed in TAP studies over this metal. Besides, the stronger adsorption of N_2O on Rh compared to Pt and Pd may favor its decomposition into N_2 and O. In this alternative pathway, N_2O would be an intermediate species in the overall reduction process NO → N_2O → N_2. Zaera and Gopinath [35] postulated that N_2O may be an intermediate species during the NO reduction to N_2 by CO over Rh(111). The dissociation of adsorbed N_2O to N_2 and O on Rh(100) has an activation energy of 8 kJ mol^{-1}, close to the 11 kJ mol^{-1} reported for the same reaction on Rh(111) [36]. Accordingly, DFT calculations suggest that secondary transformations of NO over Rh mainly lead to N_2 formation. For completeness, it should also be mentioned that the activation energy for recombination of atomic nitrogen in bridge positions leading to N_2 were 8, 44, and 31 kJ mol^{-1} for Pt(100), Pd(100), and Rh(100), respectively.

4.3. Selectivity-governing factors in ammonia oxidation

Based on TAP and DFT results, it is concluded that the three PGMs differ in the net NO selectivity due to their different reactivity towards unwanted secondary transformations of the primarily formed nitric oxide. The reduction of NO by NH_3 is particularly favored on rhodium, thus bringing the lowest NO selectivity. This conclusion is in good agreement with Pignet and Schmidt [3]. These authors assigned the lower NO selectivity over Rh to the fact that the maximum rates of the NO + NH_3 and NH_3 + O_2 reactions overlapped in temperature. Our DFT calculations make it possible to understand the differences in NO selectivity between Pt, Pd, and Rh at a molecular level. For this purpose, the following aspects were taken into consideration: (i) the surface diffusion energy of the N and O fragments to coadsorb in the same cell, (ii) the activation energies for NO formation and dissociation, and (iii) the desorption energy of adsorbed NO. The higher barrier for NO formation and lower barrier for NO dissociation over Rh(100) as well as the marked stability of adsorbed NO over rhodium make it the least selective metal for ammonia oxidation to nitric oxide. On the other extreme, platinum has the lowest barrier for NO formation, which is in line with its superior NO selectivity. Experimentally, the highest N_2O yield was found on platinum. This is tentatively attributed to the high NO coverage and the low barrier of the reaction N + NO → N_2O. For all the PGMs, the N_2O concentration at the reactor outlet decreases in ammonia excess. This is likely due to the reduction of N_2O by NH_3 leading to N_2.

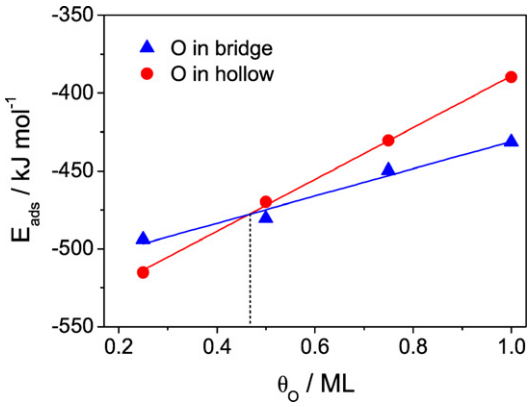

Fig. 10. Adsorption energy of atomic oxygen on bridge and hollow sites of Rh(100) as a function of the oxygen coverage.

We evidenced that an increased oxygen content in the feed suppresses loss reactions of NO with NH_3, so that ca. 100% selectivity to nitric oxide was achieved over the three PGMs at $O_2/NH_3 = 10$. On the basis of DFT, it can be put forward that a high oxygen coverage minimizes NO re-adsorption due to site blocking. To demonstrate that, the oxygen adsorption was computed as a function of the oxygen coverage on the least selective surface, Rh(100) (Fig. 10). As expected, the adsorption strength decreases with an increase of the oxygen coverage. The dependency is more pronounced for the hollow site due to the higher sharing of O with respect to the bridge site. Accordingly, at coverages higher than ca. 0.45 ML, the bridge position is the most stable adsorption site of atomic oxygen on this surface. Since NO adsorbs over bridge sites, too, its re-adsorption is hindered by adsorbed oxygen. Inderwildi et al. [37] have also shown that NO adsorption becomes weaker at higher oxygen coverage on Rh(111). Besides, in the same study, it was found that adsorbed oxygen at $\theta_O = 0.25$ inhibits the decomposition of NO molecules even though the reaction is still sterically unhindered. The activation energy of NO decomposition increased upon increasing the oxygen coverage. Other authors have also reported the severe inhibiting effect of O_2 on the NO decomposition over rhodium surfaces [31,34]. This inhibition has been explained by the electron withdrawing effect of the adsorbed oxygen, which lowers the back-donation effect of the metal into the antibonding π orbital of the end-on adsorbed NO [37]. Consequently, NO loss reactions over PGMs in general can be fully suppressed by increasing the partial O_2 pressure in the feed due to both geometric and electronic effects.

5. Conclusions

Transient studies in the TAP reactor complemented by DFT calculations provide molecular understanding of key mechanistic analogies and differences between PGM catalysts in the high-temperature ammonia oxidation. The typical ranking of NO selectivity (Pt > Pd > Rh) is mainly determined by the intrinsic reac-

tivity of the metals towards loss reactions between nitric oxide (primary product) and ammonia, leading to nitrous oxide and dinitrogen. Rhodium is the most active catalyst for the NO + NH_3 reaction, followed by palladium and platinum. The strong adsorption of NO over Rh(100) and the low barrier for NO dissociation are the main factors accounting for the experimental observations. Increasing the feed oxygen-to-ammonia ratio to 10 revealed that ca. 100% NO selectivity at a complete NH_3 conversion can be attained over Pt, Pd, and Rh. The higher the O_2/NH_3 ratio, the higher the oxygen coverage. As a result, NO dissociation is impeded and NO desorption is favored, suppressing byproduct formation. This aspect has clear practical implications taking into account that, e.g., palladium is much 4 times cheaper than platinum, the latter constituting at least 90% of the standard alloy used industrially. An optimized ammonia oxidation process can be envisaged by carefully adjusting alloy composition and oxygen content in the feed.

Acknowledgments

This research was supported by the Spanish MEC (CTQ2006-01562/PPQ, CTQU2005-08459-C02-02, and Consolider-Ingenio 2010 Grant CSD2006-0003) and the ICIQ Foundation.

References

[1] Y.M. Fogel, B.T. Nadykto, V.F. Rybalko, V.I. Shvachko, I.E. Korobchaskaya, Kinet. Catal. 5 (1964) 496.
[2] C.W. Nutt, S. Kapur, Nature 220 (1968) 697.
[3] T. Pignet, L.D. Schmidt, J. Catal. 40 (1975) 212.
[4] J.L. Gland, V.N. Korchak, J. Catal. 53 (1978) 9.
[5] M. Asscher, W.L. Gurthie, T.-H. Lin, G.A. Somorjai, J. Phys. Chem. 88 (1984) 3233.
[6] W.D. Mieher, W. Ho, Surf. Sci. 322 (1995) 151.
[7] J.M. Bradley, A. Hopkinson, D.A. King, J. Phys. Chem. 99 (1995) 17032.
[8] E. Rebrov, M.H.J.M. de Croon, J.C. Schouten, Chem. Eng. J. 90 (2002) 61.
[9] J. Pérez-Ramírez, E.V. Kondratenko, V.A. Kondratenko, M. Baerns, J. Catal. 227 (2004) 90.
[10] R. Imbihl, A. Scheibe, Y.F. Zeng, S. Günther, R. Kraehnert, V.A. Kondratenko, M. Baerns, W.K. Offermans, A.P.J. Jansen, R.A. van Santen, Phys. Chem. Chem. Phys. 9 (2007) 3522.
[11] R. Kraehnert, M. Baerns, Chem. Eng. J. 137 (2008) 361.
[12] G. Novell-Leruth, J.M. Ricart, J. Pérez-Ramírez, J. Phys. Chem. C 112 (2008) 13554.
[13] S.L. Handforth, J.N. Tilley, Ind. Eng. Chem. 26 (1934) 1287.
[14] J. Pérez-Ramírez, F. Kapteijn, K. Schöffel, J.A. Moulijn, Appl. Catal. B 44 (2003) 117.
[15] G.I. Golodets, in: Studies Surface Science Catalysis, vol. 15, Elsevier, Amsterdam, 1983, pp. 312–364.
[16] http://www.kitco.com, 19 November 2008.
[17] J. Pérez-Ramírez, E.V. Kondratenko, V.A. Kondratenko, M. Baerns, J. Catal. 229 (2005) 303.
[18] J. Pérez-Ramírez, E.V. Kondratenko, Catal. Today 121 (2007) 160.
[19] G. Kresse, J. Hafner, Phys. Rev. B 47 (1993) 558.
[20] G. Kresse, J. Furthmüller, Phys. Rev. B 54 (1996) 11169.
[21] J.P. Perdew, Y. Wang, Phys. Rev. B 45 (1992) 13244.
[22] G. Kresse, D. Joubert, Phys. Rev. B 59 (1999) 1758.
[23] R.W.G. Wyckoff, Crystal Structures, vol. 1, Wiley, New York, 1963.
[24] G. Henkelman, B.P. Uberuega, H. Jónsson, J. Chem. Phys. 113 (2000) 9901.
[25] G. Henkelman, H. Jónsson, J. Chem. Phys. 111 (1999) 7010.
[26] J.T. Gleaves, G.S. Yablonskii, P. Phanawadee, Y. Schuurman, Appl. Catal. A 160 (1997) 55.
[27] R.M. Heck, J.C. Bonacci, W.R. Hatfield, T.H. Hsiung, Ind. Eng. Chem. Process Des. Dev. 21 (1982) 73.
[28] W.K. Offermans, A.P.J. Jansen, R.A. van Santen, Surf. Sci. 600 (2006) 1714.
[29] C. Popa, R.A. van Santen, A.P.J. Jansen, J. Phys. Chem. C 111 (2007) 9839.
[30] D. Loffreda, D. Simon, P. Sautet, J. Chem. Phys. 108 (1998) 6447.
[31] D. Mei, Q. Ge, M. Neurock, L. Kieken, J. Lerou, Mol. Phys. 102 (2004) 361.
[32] G. Novell-Leruth, A. Valcárcel, J. Pérez-Ramírez, J.M. Ricart, J. Phys. Chem. C 111 (2007) 860.
[33] D. Loffreda, D. Simon, P. Sautet, J. Catal. 213 (2003) 211.
[34] G.A. Papapolymerou, L.D. Schmidt, Langmuir 1 (1985) 488.
[35] F. Zaera, C.S. Gopinath, J. Mol. Catal. A Chem. 167 (2001) 23.
[36] J.-F. Paul, J. Pérez-Ramírez, F. Ample, J.M. Ricart, J. Phys. Chem. B 108 (2004) 17921.
[37] O.R. Inderwildi, D. Lebiedz, O. Deutschmann, J. Warnatz, J. Chem. Phys. 122 (2005) 154702.